Advances in Science and Technology
Research Journal

Advances in Science and Technology Research Journal 2023, 17(2), 71–89
https://doi.org/10.12913/22998624/162104
ISSN 2299–8624, License CC-BY 4.0

Received: 2023.02.07
Accepted: 2023.03.15
Published: 2023.04.01

Modelling of Drive System Operation of a Wind Power Plant

Karol Osowski[1*], Wojciech Iwanicki[2], Jarosław Kotliński[1], Ireneusz Musiałek[2], Andrzej Kęsy[1], Zbigniew Kęsy[1]

[1] Faculty of Mechanical Engineering, Kazimierz Pulaski University of Technology and Humanities in Radom, Malczewskiego 29, 26-600 Radom, Poland

[2] University's Branch in Sandomierz, Jan Kochanowski University of Kielce, Żeromskiego 5, 25-369 Kielce, Poland

[*] Corresponding author's e-mail: k.osowski@vp.pl

ABSTRACT

The article presents experimental and theoretical studies concerning the possibility of using a controlled hydrodynamic clutch in a wind power plant's drive system. The hydrodynamic clutch is controlled by changing the distance between the hydrodynamic clutch rotors. The control system is supposed to maintain a constant angular velocity of the electric generator shaft. The considered method of control has not been used so far in power plant's drive systems. The advantages of using a controlled hydrodynamic clutch is simple structure, high durability and low weight of the entire drive system. The equations of the mathematical model for the drive system are formulated on the basis of: the balance of torques and the equations of the hydrodynamic clutch with retractable rotors. The equations are based on the one-dimensional flow of the working fluid along the mean line of the stream. The model calculations are conducted numerically. In order to be able to determine the coefficients of the mathematical model, experimental research is conducted on a test bench designed specifically for this purpose. The research determines how the rotation direction and size of the gap between rotors influences the torque transferred by the hydrodynamic clutch, for selected values of the clutch's filling degree and the working fluid's temperature. On the basis of the model calculations results it was determined that a hydrodynamic clutch controlled by increasing the distance between rotors may be successfully used in drive systems of wind power plants to maintain a constant angular velocity of the electric generator shaft.

Keywords: hydrodynamic clutches, drive systems, hydrodynamic clutch tests, wind power plant.

INTRODUCTION

The latest tendency of the development of power engineering is the use of distributed energy resources characterized by a large number of equally distributed sources generating small scale power [1]. They may be various renewable energy sources using sun, water or wind. Among these sources, the most popular is a small scale wind power [2–6].

Small scale wind power plants are usually built using a wind turbine, a gearbox, an electric current generator, and a brake [7]. Due to the changing demand for electricity, it is necessary to create an energy storage for wind power plants. There are different energy storage technologies, including e.g.: battery energy storage systems, hydrogen-based energy storage systems and flywheel energy storage systems [8, 9]. If the electric energy obtained from a power plant is not stored, then it is vital for the power generator to produce electrical current whose parameters meet requirements of local power grids. A current with a specified frequency can be obtained in a power plant electrically, using power electronics converters, or mechanically, by adjusting the angular velocity of the wind turbine shaft [7, 10]. The over speed control mechanisms of wind turbines are pitch-to-stall rotors, coning rotors and rotors with deformable blades. In turn, controlling the angular velocity of the generator shaft can be managed by controlling the inertia of a wind turbine rotor [11], a flywheel energy storage system [12] or hydrodynamic drive systems [13].

In wind power plants, using hydrodynamic elements, such as clutches, torque converters and brakes, is justified by the fact that they are machine components with high durability. Increasing the durability of drive systems is currently one of the most fundamental directions of developmental works concerning wind power plants [14, 15]. In turn, weight is highly important in high-altitude wind power plants placed in balloons or kites [16]. *WinDrive* [17] is a hydrodynamic drive system currently used to maintain a constant angular velocity of the generator shaft with varying rotations of the wind turbine. It consists of a hydrodynamic torque converter controlled by rotating blades of a fixed rotor of a stator, and two planetary gears. One of the planetary gears is used to split the power stream; one part of the stream flows through the hydrodynamic torque converter, while the other flows through the mechanical gear. This increases the efficiency of the hydrodynamic drive system.

Other, less complicated and often employed means of controlling the hydrodynamic components are: throttling to change the flow rate of the working fluid, changing the filling degree of the working space with a working fluid, or attaching an additional rotor to the torque converter during its operation [18-21]. The newest means of controlling hydrodynamic components rely on the use of so-called intelligent fluids, electrorheological fluids or magnetorheological fluids in which shear stress values change after exposure to electric or magnetic field respectively [22-24]. There is also research conducted to determine how 3D-printed rotors with deformable blades can be used to control hydrodynamic components [25-27].

Different mathematical models are used to model hydrodynamic components: one-dimensional models (1D) [28-30], two-dimensional models (2D) [31, 19] and three-dimensional models (3D) [32-35]. 1D mathematical models are most commonly used models, due to their simplicity, the capability to easily formulate dynamic equations describing transient motion of the hydrodynamic drive system and the possibility to use them in initial stages of theoretical research. These models do not demand determining all the dimensions of the hydrodynamic component (which is necessary for 2D and 3D models) [36-38]. In 1D models, high accuracy is obtained by determining the numerical coefficients of the model through experimental research [39, 40]. Because of that, the 1D models' accuracy is similar to the accuracy of the more complex 2D and 3D models [31, 42]. Multiple-stream models are also created based on 1D models, and they are used for multi-criteria optimization of hydrodynamic elements [43].

The purpose of the paper is modelling the operation of a wind power plant intended for a distributed energy system with a hydrodynamic drive system in which a hydrodynamic clutch (HC) with sliding rotors is used to control the rotational speed of the generator. The described research contributes to increasing the level of knowledge about hydraulic drive systems of machines by developing and testing of a new method of HC control by sliding rotors. Until now, such a control method has not been deemed efficient

Nomenclature	
HC	hydrodynamic clutch
a, b, c, d, e, f	numerical coefficients
c_m	meridional velocity
c_u	peripheral speed
g	gravitational acceleration
h	gap size
h_1	pump head rise
h_2	turbine head rise
i	gear ratio for the gearbox
i_k	speed ratio
t	time
u	lifting speed
w	relative speed
J	mass moments of inertia
F_m	meridional cross-section
M_1	torque transferred by hydrodynamic clutch
M_e	torque obtained from experiment
M_h	braking torque
M_r	motion resistance torque
M_s	driving torque
P	mechanical power
Q	flow rate of working fluid
β	angle between relative speed and lifting direction
ε	reduction coefficient
φ	rotor friction loss coefficient
ρ	density of the working fluid
ρ_3	radius ratio
ω_1	angular velocity of input shaft
ω_2	angular velocity of output shaft
σ	linear speed ratio

enough to be developed and tested. However, in machine drive systems where the energy losses are less important (such as generator drive in a wind power plant) this solution can be successfully applied. In order to achieve the assumed goal, it was necessary to develop testing methodology for a prototype design solution of a wind power plant with a hydrodynamic drive system, to develop a specialized test stand and to derive a new mathematical model taking into account the flow in HC with an enlarged gap between the rotors. The advantages of using a controlled hydrodynamic clutch is simple structure, high durability and low weight of the entire drive system. The obtained results of both theoretical and experimental research allow to determine the performance characteristics, the range of control and to compare this control method with other methods currently used in wind power plants.

CONCEPT FOR CONSTRUCTION AND OPERATION OF A WIND POWER PLANT WITH A HYDRODYNAMIC CLUTCH

A low-power wind power plant was selected to research the method of controlling the hydrodynamic drive system of a wind power plant by sliding HC turbine rotor, the diagram of which is shown in Figure 1.

Table 1. Technical data of the wind power plant's generator

Type	Power	Nominal working conditions
DC motor Multimoto G 11.05	5.5 kW	ω_n = 150 rad/s, U_n = 400 V, I_n = 15.4 A

It is assumed, that due to the requirements of a local power grid, the wind power plant generator operates with angular velocity ω_2 = 150 rad/s. It supplies electrical current with a frequency of 50 Hz and constant power regardless of wind speed changes, and thus regardless of the angular velocity of the power plant's rotor ω_w. The technical data of the generator are shown in Table 1, in which the nominal parameters are marked with the index n.

The drive system of the generator comprises a mechanical gearbox which increases the rotor speed, and a HC consisting of rotors with variable blade geometry. Using rotors with blades shaped in this manner allowed to obtain two different characteristics when changing the rotation direction of the pump rotor. The clutch operated with a constant filling degree ψ, determined as the ratio of the working fluid's volume in the working space to the entire volume of this space. The HC data is shown in Table 2. Figure 2 presents photos of the HC rotors.

The principle of operation of the drive system of a generator whose HC is controlled by sliding rotors is based on changing the torque transferred by the clutch. It is illustrated in Figure 3, on the basis of the HC characteristics in the following form: $M = f(\omega_2)$.

Under nominal conditions of the generator's operation (point A in Fig. 3), the turbine operates, as intended, with angular velocity ω_{2A} = 150

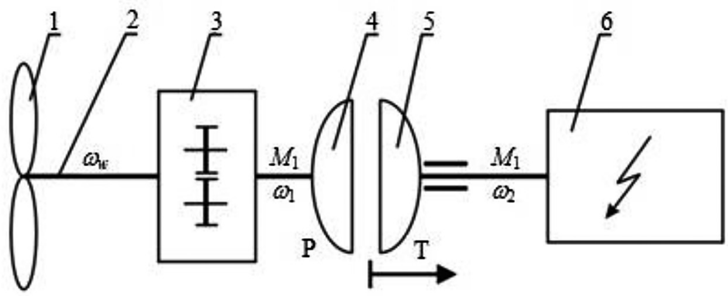

Fig. 1. Scheme of the power plant with a HC controlled by sliding HC turbine rotor: 1 – wind turbine rotor, 2 – drive shaft, 3 – gearbox, 4 – HC pump rotor, 5 – HC turbine rotor, 6 – generator

Table 2. Values of angles and radii on the mean line of rotors of the HC prototype

Rotor rotation direction	β_{11} [°]	β_{12} [°]	β_{21} [°]	β_{22} [°]	r_1 [mm]	r_2 [mm]	Number of blades
Left	118	65	59	137	65.9	115.3	39
Right	62	115	121	43			

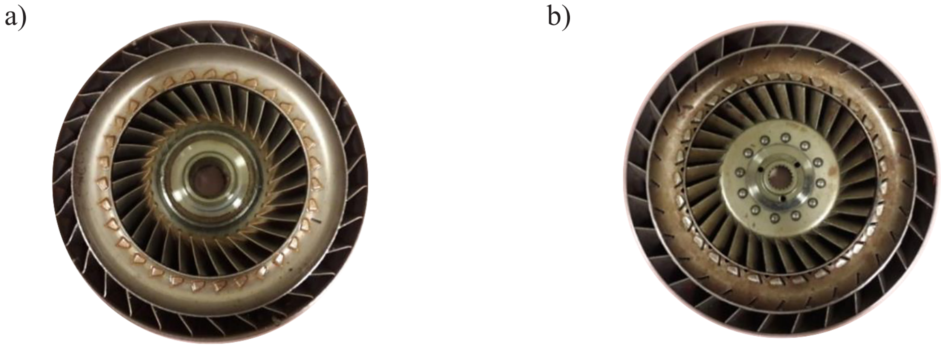

Fig. 2. View of the HC rotors: a – the pump, b – the turbine

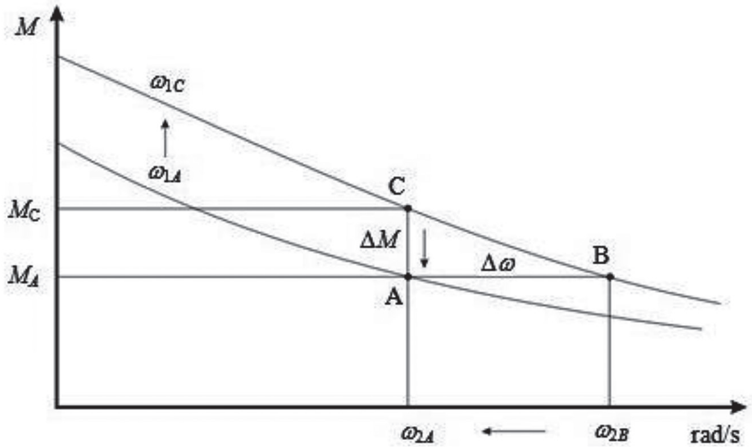

Fig. 3. Illustration of the principle of operation of the drive system of a generator whose HC is controlled by increasing the distance between rotors

rad/s. The torque transferred by the HC is M_A. The wind power plant's rotor rotates with the constant angular velocity ω_{w1}, and the HC pump operates with angular velocity ω_{1A}, wherein the dependence $\omega_{1A} = i \cdot \omega_{w1}$ is maintained. Then, the kinematic ratio of the HC is $i_{kA} = \omega_{2A}/\omega_{1A}$,and the HC efficiency is $\eta_A = i_{kA}$. If the wind speed increases, the wind power plant's rotor rotates with angular velocity ω_{w2}, and the angular velocity of the HC pump's angular velocity increases to $\omega_{1C} = i \cdot \omega_{w2}$. This causes an increase in the torque value to M_C. The angular velocity of the turbine's rotor increases by $\Delta\omega$ up to the speed $\omega_{2B} > \omega_{2A}$. In order to decrease the angular velocity ω_{2B} to the angular velocity ω_{2A} the rotors move away. This causes a decrease in the value of the torque transferred by the HC, up to the point when ω_{2B} reaches the nominal value ω_{2A}. The HC pump still operates with rotational speed ω_{1C}, but as a result of moving the rotors aside, the torque decreases from M_C by ΔM, and its value returns to M_A. The turbine operates again in point A, but now $i_{kC} = \omega_{w2}/\omega_{1C}$, wherein $i_{kC} < i_{kA}$, and thus $\eta_C < \eta_A$. As a result of moving aside the HC rotors, despite an increase in the wind speed, the operation parameters of the generators are not changed, but the drive system of the generator works less efficiently.

If the wind speed increases significantly and exceeds the safe value (above which the failure of the wind farm may occur) then the shaft of the wind power plant's rotor is braked or immobilized. A HC may be used for this purpose, operating as a controlled brake. Figures 4 and 5, on the basis of the data from Table 3, illustrate the result

Table 3. Data and calculation results from the drive system containing a HC controlled by increasing the distance between rotors

ω_w [rad/s]	i [-]	ω_2 [rad/s]	M_A [Nm]	P [kW]	ω_1 [rad/s]	h [mm]	i_k [-]	η [-]
1.5	125	150	18	2.8	187.5	0	0.8	0.8
2.0					250.0	58	0.6	0.6

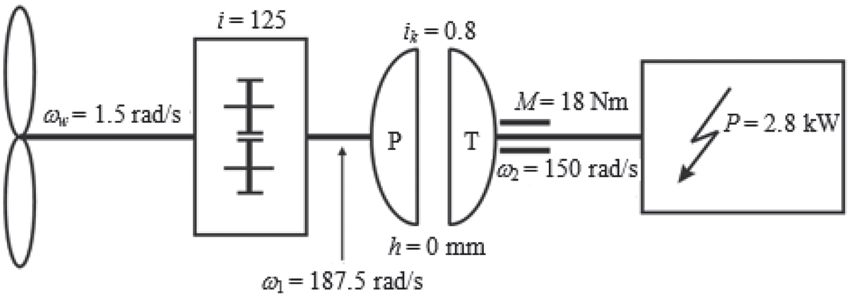

Fig. 4. Operation parameters of the power plant's drive system – initial conditions

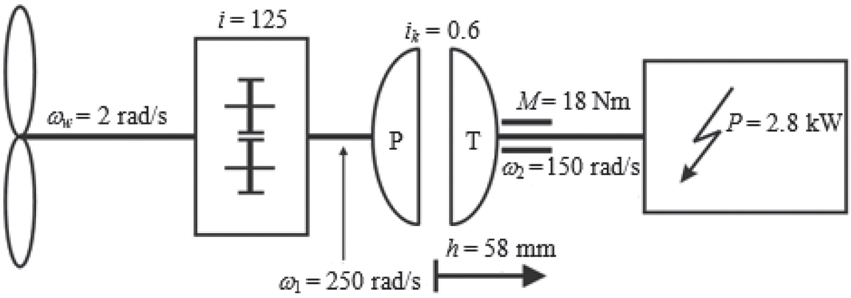

Fig. 5. Operation parameters of the power plant's drive system – final conditions

of the control method of the hydrodynamic drive system of a wind turbine generator containing a HC with sliding turbine rotor.

As shown in Figures 4 and 5, despite an increase in the angular velocity ω_w, the angular velocity ω_2 does not change.

A SIMULATION OF THE WIND POWER PLANT'S OPERATION

Mathematical model of the hydrodynamic drive system of the wind power plant

What is considered in modelling the dynamics of the drive system of wind power plants, is the balance of torques affecting the shafts of the drive system components, taking into account the moments of inertia [43-45]. In considerations concerning the modelling of a transient motion of a hydrodynamic drive system containing a HC, it is assumed, for the sake of simplicity, that changes in angular velocity ω with time are caused only by the presence of inertial masses. The remaining torques are the same as in the case of a steady motion [46, 47]. Additionally, the shafts' stiffness is omitted. The formulas of mathematical model for a drive system with a HC are formulated after dividing the drive system into two sections: the driving part and the driven part, the two connected with a working fluid [48, 49]:

$$
\begin{aligned}
M_s &= M_1 + J_1 \frac{d\omega_1}{dt} \\
M_r &= M_1 - J_2 \frac{d\omega_2}{dt}
\end{aligned}
\tag{1}
$$

where: M_s – driving torque, M_1 – torque transferred by the HC, M_r – motion resistance torque, J_1, J_2 – mass moments of inertia, reduced for the driving and driven shafts respectively, ω_1 – angular velocity of the HC input shaft, ω_2 – angular velocity of the HC output shaft.

These equations are first-order nonlinear differential equations whose solutions demand using numerical methods. The torque M_1 is calculated on the basis of a 1D medium stream model widely used in calculations of hydrodynamic elements [50-52]. Figure 6 depicts the HC scheme used to derive equations of the model.

The points 11 and 22 signifying the inlet of the pump and the outlet of the turbine rotor are located on the radius r_1. The points 12 and 21, respectively, are located on the radius r_2. In this designation, the first number signifies the rotor (1 – pump, 2 – turbine), and the second – an inlet (number 1) and outlet (number 2). Figure 7 shows the distribution of the absolute speed c of the fluid flowing in the channel of the hydrodynamic component's rotor.

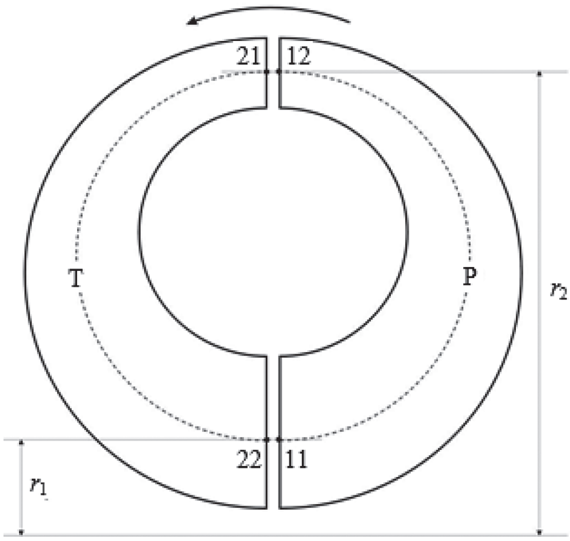

Fig. 6. Meridional cross-section of the HC: P – pump rotor, T – turbine rotor

The HC rotors' torque is caused by the peripheral speed c_u, so the hydraulic torques M of the HC pump rotor and the HC turbine rotor are equal, as follows [53, 54]:

$$M_1 = \rho Q\,[c_{u12}r_2 - c_{u11}r_1] \tag{2}$$

where: Q – flow rate of the working fluid, ρ – density of the working fluid, c_{u11} – peripheral speed at the inlet of the pump rotor, c_{u12} – peripheral speed at the outlet of the pump rotor.

It is assumed that the absolute speed at the inlet of the examined rotor is equal to the absolute speed at the outlet of the previous rotor, which also means that the peripheral speeds c_u are equal. On this basis, in formula (2), it is taken into account that:

$$c_{u11} = c_{u22}\,,\; c_{u21} = c_{u12} \tag{3}$$

where: c_{u21} – peripheral speed at the inlet of the turbine rotor, c_{u22} – peripheral speed at the outlet of the turbine rotor, thus:

$$M_1 = \rho Q\,[c_{u12}r_2 - c_{u22}r_1] \tag{4}$$

Head rise balance of the pump rotor h_1 and the turbine rotor h_2 can be determined on the basis of the following equations:

$$h_n = \frac{M_1\omega_n}{\rho g Q} = \frac{\omega_n}{g}(c_{un2}r_2 - c_{un1}r_1)$$
$$c_{un2} = u_{n2} + c_m ctg\beta_{n2}\,,\; c_{un1} = u_{n1} + c_m ctg\beta_{n1} \tag{5}$$

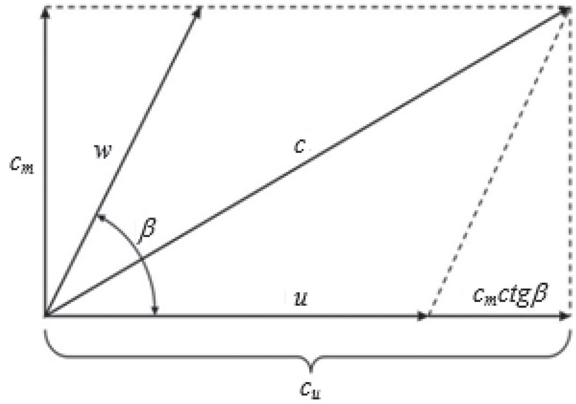

Fig. 7. Distribution of the speed of the fluid flowing in the HC rotor channel: u – lifting speed, w – relative speed, c_u – peripheral speed, c_m – meridional velocity, β – angle between relative speed and lifting direction

where: $n = 1$ for the pump rotor, $n = 2$ for the turbine rotor, g – gravitational acceleration.

Head rise balances take the following form:

$$h_1 = \frac{\omega_1}{g}[(u_{12} + c_m ctg\beta_{12})r_2 - (u_{22} + c_m ctg\beta_{22})r_1]$$
$$h_2 = -\frac{\omega_2}{g}[(u_{12} + c_m ctg\beta_{12})r_2 - (u_{22} + c_m ctg\beta_{22})r_1] \tag{6}$$

After introducing dimensionless parameters:

$$\sigma = \frac{\omega_1 r_2}{c_m} = \frac{u_{12}}{c_m}\,,\; \rho_3 = \frac{r_1}{r_2}\,,\; i_k = \frac{\omega_2}{\omega_1} \tag{7}$$

where: σ – linear speed ratio, ρ_3 – radius ratio, i_k – speed ratio,

formulas (6) are written as follows:

$$h_1 = \frac{\omega_1 r_2}{g}[(u_{12} + c_m ctg\beta_{12}) - (u_{22} + c_m ctg\beta_{22})\rho_3]$$
$$h_2 = -\frac{\omega_1 i_k r_2}{g}[(u_{12} + c_m ctg\beta_{12}) - (u_{22} + c_m ctg\beta_{22})\rho_3] \tag{8}$$

Formula (8) shows that $h_2 = h_1 i_k$.

The first equation of system of equations (8) is introduced on the basis of the formula $u = wr$, the dependence:

$$u_{12} = \omega_1 r_2\,,\; u_{22} = \omega_2 r_1 = \omega_1 i_k r_2\,,\; \rho_3 = u_{12} i_k \rho_3 \tag{9}$$

Dividing both sides of the obtained equation by $c_m^{\,2}$ and then multiplying both sides by $2g$, gives the following result:

$$\frac{2h_1 g}{c_m^{\,2}} = \frac{2\omega_1 r_2}{c_m}\left[\frac{u_{12}}{c_m} + \frac{u_{12}}{c_m} i_k\rho_3 + ctg\beta_{12} - ctg\beta_{22}\rho_3\right] \tag{10}$$

or, after introducing the designation:

$$\sigma = \frac{\omega_1 r_2}{c_m} = \frac{u_{12}}{c_m}$$

$$\frac{2h_1 g}{c_m^{\ 2}} = 2\sigma^2(1 - i_k\rho_3) + 2\sigma(ctg\beta_{12} - ctg\beta_{22}\rho_3) \quad (11)$$

equation (11) can be formed as follows:

$$\begin{gathered} \frac{2h_1 g}{c_m^{\ 2}} = a_h\sigma^2 + b_h\sigma \\ a_h = 2(1 - i_k\rho_3) \\ b_h = 2(ctg\beta_{12} - ctg\beta_{22}\rho_3) \end{gathered} \quad (12)$$

In the HC head rise, factors taken into account are the losses of friction of the liquid against the walls of the rotor channels and the losses of the impact of the liquid flowing into the rotors against the blades. The friction losses h_t are calculated on the basis of relative speeds w at the rotors' output:

$$\begin{gathered} w_{12} = \frac{c_m}{\sin\beta_{12}} = c_m\sqrt{ctg^2\beta_{12} + 1}\,, \\ w_{22} = \frac{c_m}{\sin\beta_{22}} = c_m\sqrt{ctg^2\beta_{22} + 1} \end{gathered} \quad (13)$$

according to the formula:

$$h_t = \varphi\frac{w_{12}^{\ 2}}{2g} + \varphi\frac{w_{22}^{\ 2}}{2g} \quad (14)$$

the result is:

$$h_t = \varphi\frac{c_m^{\ 2}}{2g}(ctg^2\beta_{12} + ctg^2\beta_{22} + 2) \quad (15)$$

where: φ – rotor friction loss coefficient, which is a function of i_k, w_{12} – relative speed at the outlet of the pump rotor, w_{22} – relative speed at the outlet of the turbine rotor.

The research shows that the Reynolds number in the rotors of the hydrodynamic torque converters and hydrodynamic clutches ranges from 10^4 to 10^6 [28, 32]. Therefore, to determine the friction loss coefficient φ (when it is not determined experimentally) turbulent flow formulas are used, e.g. Blasius formula [49-52]. Division of equation (15) on both sides by $c_m^{\ 2}$ and its multiplication by $2g$ resulted in the following equation:

$$\frac{2h_t g}{c_m^{\ 2}} = \varphi(ctg^2\beta_{12} + ctg^2\beta_{22} + 2) \quad (16)$$

Equation (16) may be written as:

$$\begin{gathered} \frac{2h_t g}{c_m^{\ 2}} = c_t \\ c_t = \varphi(ctg^2\beta_{12} + ctg^2\beta_{22} + 2) \end{gathered} \quad (17)$$

Impact losses h_u are determined with the formula:

$$h_u = \frac{c_{u1}^{\ 2}}{2g} + \frac{c_{u2}^{\ 2}}{2g} \quad (18)$$

wherein:

$$\begin{gathered} c_{u1} = c_{u11} - c_{u22} = u_{11} + c_m ctg\beta_{11} - u_{22} - c_m ctg\beta_{22} \\ c_{u2} = c_{u21} - c_{u12} = u_{21} + c_m ctg\beta_{21} - u_{12} - c_m ctg\beta_{12} \end{gathered} \quad (19)$$

where: c_{u1}– speed of the working fluid hitting the blades at the inlet of the pump rotor, c_{u2} – speed of the working fluid hitting the blades at the inlet of the turbine rotors.

Taking into account the following dependencies in equations (19):

$$\begin{gathered} u_{11} = \omega_1 r_1 = \omega_1\rho_3 r_2 = u_{12}\rho_3 \\ u_{21} = \omega_2 r_2 = \omega_1 i_k r_2 = u_{12} i_k \\ u_{22} = \omega_2 r_1 = \omega_1 i_k r_1 = u_{12} i_k\rho_3 \end{gathered} \quad (20)$$

leads to the following equations:

$$\begin{gathered} c_{u1} = c_{u11} - c_{u22} = u_{12}\rho_3 + c_m ctg\beta_{11} - u_{12} i_k\rho_3 - c_m ctg\beta_{22} \\ c_{u2} = c_{u21} - c_{u12} = u_{12} i_k + c_m ctg\beta_{21} - u_{12} - c_m ctg\beta_{12} \end{gathered} \quad (21)$$

After substituting formulas (18) to formulas (21), and then dividing both sides of the received equation by $c_m^{\ 2}$ and multiplying both sides by $2g$, the result is as follows:

$$\begin{gathered} \frac{2h_u g}{c_m^{\ 2}} = (\delta\rho_3 + ctg\beta_{11} - \delta i_k\rho_3 - ctg\beta_{22})^2 + (-\delta + \delta i_k + ctg\beta_{21} - ctg\beta_{12})^2 \\ = \delta^2(\rho_3 - i_k\rho_3)^2 + 2\delta[(\rho_3 - i_k\rho_3)(ctg\beta_{11} - ctg\beta_{22}) + (i_k - 1)(ctg\beta_{12} - ctg\beta_{21})] \\ + (ctg\,\beta_{11} - ctg\,\beta_{22})^2 + (ctg\,\beta_{21} - ctg\,\beta_{12})^2 \end{gathered} \quad (22)$$

Formula (22) can be written as:

$$\frac{2h_u g}{c_m^{\ 2}} = a_u\delta^2 + b_u\delta + c_u \quad (23)$$

where:

$$\begin{gathered} a_u = (\rho_3 - i_k\rho_3)^2 \\ b_u = 2[(\rho_3 - i_k\rho_3)(ctg\beta_{11} - ctg\beta_{22}) + (i_k - 1)(ctg\beta_{12} - ctg\beta_{21})] \\ c_u = (ctg\beta_{11} - ctg\beta_{22})^2 + (ctg\beta_{21} - ctg\beta_{12})^2 \end{gathered} \quad (24)$$

The head rise balance equation is written as:

$$h_1 - h_1 i_k - h_u - h_t = 0 \quad (25)$$

After substituting the head rise balance formulas represented by equations (12), (17), (23) to equation (25), and after dividing both sides of the obtained equation by $c_m^{\ 2}$ and multiplying both sides of the equation by $2g$, a quadratic equation is obtained with regard to the parameter σ, in the following form:

$$a\sigma^2 + b\sigma + c = 0$$
$$a = a_h(1 - i_k) - a_u \tag{26}$$
$$b = b_h(1 - i_k) - b_u \quad c = -c_u - c_t$$

where: a, b, c – coefficients of the quadratic equation with respect to the parameter σ.

After assigning numerical values to the coefficients of equation (26), the solved equation allows to calculate the value of the σ parameter, wherein a positive value of the parameter σ is assumed for the following calculations.

Values of the torque M_1, are calculated after transforming formula (5) from the dependence:

$$M_1 = \frac{h_1 \rho g Q}{\omega_1} \tag{27}$$

where: h_1 – the pump head rise calculated for a known value of the parameter σ.

In a HC with sliding rotors, when a gap is created between the rotors of the pump and the rotors of the turbine, the fluid stream Q is split. A part of the stream flows out through the gap between rotors and does not enter the turbine's rotor. Due to that, a flow rate reduction coefficient ε is introduced. The coefficient is dependent on the width of the gap between rotors h. It is assumed that:

$$Q = c_m F_m \varepsilon \tag{28}$$

where: F_m – meridional cross-section of the rotor's channel, c_m – meridional speed.

The fluid stream flowing out through the gap flows around the turbine, transferring some of its energy to the turbine, so the gap's presence does not have a significant influence on the HC characteristics. Due to that, in the following calculations concerning the HC with sliding rotors, it is arbitrarily assumed, that the flow rate reduction coefficient is a function of the gap width h and i_k:

$$\varepsilon = f(h, i_k) \tag{29}$$

wherein, for $h = 0$ and $i_k = 0$ the coefficient $\varepsilon = 1$, and it decreases to 0 with an increasing h, so the coefficient $\varepsilon \leq 1$.

On the basis of formulas (27), (28), the following was obtained:

$$M_1 = \frac{\rho g F_m}{\omega_1} c_m h_1 \varepsilon \tag{30}$$

Substituting the meridional velocity c_m described by formula (7) and head rise balance h_1 described by formula (8) into relation (30), finally, the formula for the torque transferred by the HC, in the following form:

$$M_1 = \rho F_m \omega_1^2 r_2^3 \frac{\sigma(1 - \rho_3^2 i_k) + ctg\beta_{12} - \rho_3 ctg\beta_{22}}{\sigma^2} \tag{31}$$

Experimental determination of the coefficients of the mathematical model

Performing calculations based on the presented mathematical model of a hydrodynamic clutch with sliding rotors requires the determination of the geometric parameters of the HC, such as: radii r_1 and r_2, the angles of the pump rotor blades β_{11} and β_{12}, the angles of the turbine rotor blades β_{21}, β_{12}, and two coefficients: the friction loss coefficient φ and the flow rate reduction coefficient ε. The geometrical parameters of the HC are obtained on the basis of rotor measurements or from the technical documentation, whereas determining the coefficients φ and ε demands conducting experimental research. As a result, the coefficients are presented as polynomials.

In order to assess the correctness of the mathematical model of the examined HC, the model is verified by comparing the results of numerical calculations with the results of experimental research obtained for selected measurement points. The criteria assumed for correctness assessment are relative errors δ_M [%] and absolute errors Δ_M [Nm] described by the following formulas:

$$\Delta_M = |M_e - M_t| \tag{32}$$

$$\delta_M = \frac{\Delta M}{M_e} \cdot 100\% \tag{33}$$

where: M_e – torque measured during experimental research, M_t – torque obtained as a result of numerical calculations on the basis of the mathematical model.

The experimental research concerning determination of coefficients ε and φ are conducted on a test bench built specifically for this purpose. The test bench consists of: an AC drive motor, a generator, a control system, a rotor sliding mechanism with an electric actuator, and a computer measurement system registering measurement data in real time [55]. The scheme of the test bench is shown in Figure 8.

In order to simplify the construction of the test bench, the HC rotors are set directly on the shafts of the AC drive motor and the generator, and the sliding of the rotors is carried out by horizontal movement of the generator on the ways attached to the test bench frame. The turbine's rotor is placed on the generator's shaft. The drive motor and the brake are controlled by Emerson's AC Drive and DC Drive control systems. The performance of the systems is overviewed by the PLC driver cooperating with encoders attached to the shafts of electric drive motors. The basic data of the components of the test bench are presented in Table 4.

The computer measuring system is integrated with the electric control system of the test bench. During the measurements of torque *M* and angular velocities of the electric drive system shaft ω_1 and of the generator shaft ω_2, the values are retrieved from the PLC driver, and subsequently recorded using a PC with a specialized software. During the experimental research with the HC output shaft stopped, a strain gauge force sensor is used to measure the torque. The strain gauge force sensor used is the KM 102 K with a measuring range from 0 to 500 N. The value of the recorded force is read using a digital measuring indicator MD 150T. The temperature of the working fluid is measured by a Heraeus M222 temperature sensor from Conrad Electronic. The accuracy of the measurements is presented in Table 5.

The experimental research is conducted for working fluid temperatures occurring in HCs operating within machine's drive systems. However, the HC heats up rapidly during the test bench research, so the measurements are performed not for constant, selected temperature values, but for two temperature ranges: from 40 ˚C to 50 ˚C and from 80 ˚C to 90 ˚C. In order to increase the credibility of the research results, the measurements are repeated several times, discarding extreme results, while the remaining results are averaged.

Calculating the coefficient φ

The coefficient φ is calculated numerically on the basis of the presented HC mathematical model, based on the characteristics $M_e = f(i_k)$ for

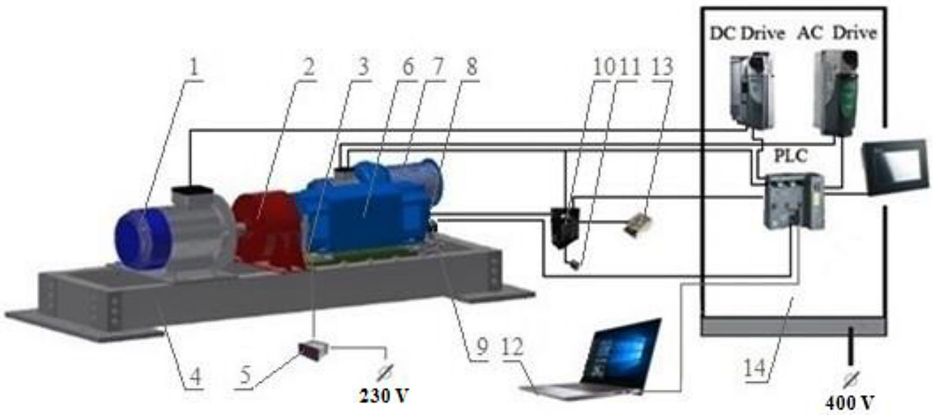

Fig. 8. Test bench scheme: 1 – AC drive motor, 2 – examined HC, 3 – temperature sensor, 4 – frame, 5 – digital temperature indicator, 6 – generator placed on ways, 7 – generator's cooling system, 8 –encoder, 9 – electric actuator, 10 – electric actuator controller, 11 – actuator direction switch, 12 – PC, 13 –12V power supply, 14 – control cabinet

Table 4. Component data of the test bench used to assess the HC

Usage	Model/ type	Current type	Parameter values
AC drive motor	Tamel 3SG132S-4-IE2 5.5 kW	AC	ω =146 rad/s U_n = 400 V
PLC driver	Siemens Simatic DP 6ES7151-8AB01-0AB0	AC	U = 230 V
AC Drive control system	Emerson Unidrive SP 1406	AC	U_n = 400 V
DC Drive control system	Emerson Mentor MP 25A4R	AC	U_n = 400 V

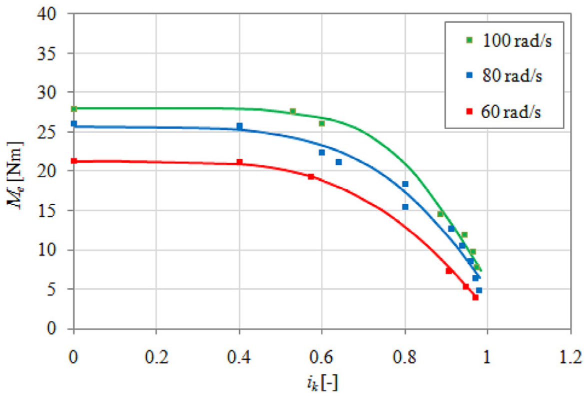

Fig. 9. Dependence $M_e = f(i_k)$ for ψ = 92%, T_2 = 60 - 80˚C, different angular velocities of the pump rotor ω_1 and left-hand rotation direction of the HC pump rotor

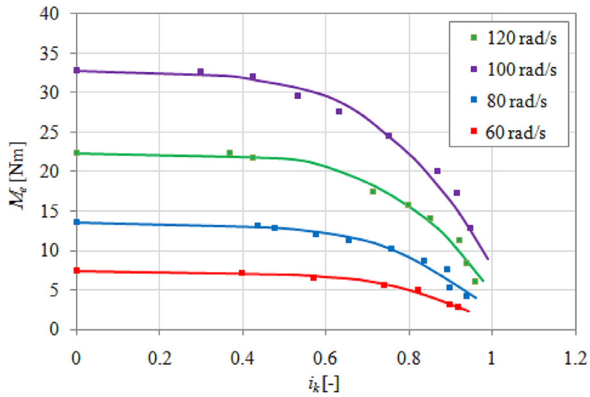

Fig. 10. Dependence $M_e = f(i_k)$ for ψ = 92%, T_2 = 60 - 80˚C, different angular velocities of the pump rotor ω_1 and right-hand rotation direction of the HC pump rotor

ω_1 = const. obtained from the HC experimental research, presented in Fig. 9 and Fig. 10.

The calculations are conducted in the following manner: for a selected point (M_e, i_k) obtained from the charts presented in Fig. 9 and Fig. 10 and the rotational speed ω_1 = const., friction losses are calculated using dependence (15) and dependence (31), and subsequently the function $\varphi = f(i_k)$ is created for a selected angular velocity ω_1, Table 6.

In the HC mathematical model, according to mean streamline theory, it is assumed that the friction loss coefficient φ is a function of i_k and is not dependent on angular velocities of the rotors. This is why, on the basis of the equations shown in Table 6, the course of $\varphi_{av} = f(i_k)$ is determined for both directions of rotation of the pump rotor, Table 7.

Table 5. Accuracy of the measurements. performed on the test bench

Measured quantity	Relative measurement error
h	2 %
ω_1, ω_2	2 %
M	5 %
T	1 %

Table 6. Equations describing dependencies $\varphi = f(i_k, \omega_1)$ for different ω_1 values

Rotation direction	ω_1 value [rad/s]	Equation $\varphi = f(i_k, \omega_1)$
Left	100	$\varphi = 20.73\ i_k^2 - 42.13\ i_k + 23.23$
	80	$\varphi = 9.77\ i_k^2 - 21.34\ i_k + 12.67$
	60	$\varphi = 6.66\ i_k^2 - 1.72\ i_k + 7.19$
Right	120	$\varphi = 17.79\ i_k^2 - 28.38\ i_k + 12.32$
	100	$\varphi = 21.85\ i_k^2 - 33.05\ i_k + 13.47$
	80	$\varphi = 24.49\ i_k^2 - 36.85\ i_k + 15.57$
	60	$\varphi = 26.67\ i_k^2 - 40.34\ i_k + 17.2$

Table 7. Equations describing the dependencies $\varphi_{av} = f(i_k)$

Rotation direction	Equation $\varphi_{av} = f(i_k)$
Left	$\varphi_{av} = 12.39\ i_k^2 - 25.41\ i_k + 14.36$
Right	$\varphi_{av} = 22.70\ i_k^2 - 34.65\ i_k + 14.64$

Table 8. Relative error and absolute error for ω_1= 100 rad/s and left-handed rotations of the pump rotor

ω_1 [rad/s]	i_k	M_e [Nm]	M_t [Nm]	Δ_M [Nm]	δ_M [%]
100	0.98	6.12	5.44	0.68	11.10
	0.97	7.72	6.90	0.82	10.61
	0.96	9.77	8.22	1.55	15.91
	0.94	11.80	10.60	1.20	10.15
	0.89	14.50	15.82	1.32	9.09
	0.53	27.50	34.54	7.04	25.61
	0.00	28.00	37.67	9.62	34.31
	average	value		3.18	16.68

The correctness assessment of the friction loss coefficient's φ values are performed on the basis of errors Δ_M and δ_M obtained for the torque values M_e and torque values M_t. These values are calculated on the basis of mathematical model equations, using the dependences $\varphi_{av} = f(i_k)$ presented in Table 7. The calculations are conducted numerically, for the gap size h = 0. The results of the calculations are juxtaposed in Table 8 (for left-handed pump rotor's rotations) and in Table 9 (for right-handed pump rotor's rotations).

Calculating the coefficient ε

The coefficient ε is calculated numerically on the basis of the presented HC mathematical model, based on the characteristics $M_e = f(i_k)$ for h = const.. The characteristics are obtained from the HC experimental research, presented in Fig. 11 and Fig. 12. In order to obtain the values of the coefficient $\varepsilon \leq 1$, the subsequent values of the torque M_e for $i_k > 0$ and $h > 0$ are divided by the highest value of the torque M_e occurring for i_k = 0 and h = 0.

In the mathematical model of the HC with sliding rotors, it is arbitrarily assumed that the flow rate reduction coefficient ε is a function of the gap h and the kinematic ratio i_k. It is not dependent on the rotors' angular velocities. However, on the basis of the analysis of the results of the initial experimental research, it is determined that the value of the coefficient ε is also slightly dependent on angular velocities ω_1. Due to that, the course of the dependence $\varepsilon = f(h, i_k)$ is determined in two stages, in a similar manner to how the coefficient φ is determined.

The first stage, on the basis of the measuring points' coordinates obtained from HC characteristics experimental research, determines the dependences $\varepsilon = f(h, i_k)$ for selected values of the pump rotor's angular velocities ω_1 = const., both for left-hand and right-hand rotations. For instance, the coefficient ε values for ω_1 = 100 rad/s obtained in such manner are presented as charts in Fig. 13 and Fig. 14.

The second stage of the calculations of the coefficient ε determines the course of $\varepsilon_{av} = f(h, i_k)$ for

Table 9. Relative error and absolute error for ω_1= 100 rad/s and right-handed rotations of the pump rotor

ω_1 [rad/s]	i_k	M_e [Nm]	M_t [Nm]	Δ_M [Nm]	δ_M [%]
100	0.96	6.06	6.07	0.01	0.16
	0.94	8.47	7.54	0.93	10.95
	0.92	11.40	8.85	2.55	22.36
	0.85	13.86	12.72	1.14	8.23
	0.80	15.67	14.93	0.74	4.75
	0.72	17.56	17.49	0.07	0.38
	0.42	21.68	20.71	0.97	4.46
	0.37	22.26	20.87	1.39	6.26
	0.00	22.34	21.75	0.59	2.66
	average	value		0.93	6.69

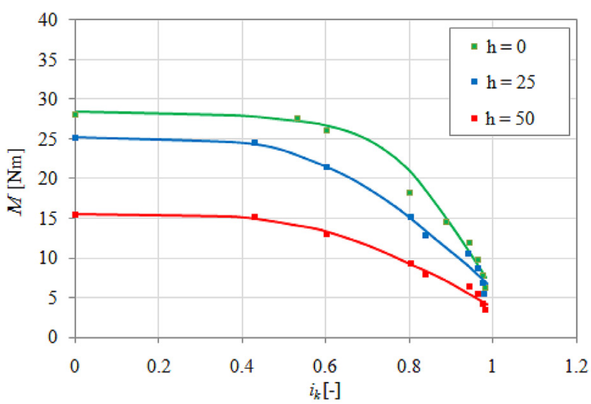

Fig. 11. Dependence $M = f(i_k)$ for the gap $h > 0$, filling degree ψ = 92%, temperature T_2 = 60 - 80°C, velocity ω_1= 100 rad/sand left-hand rotations of the HC pump rotor

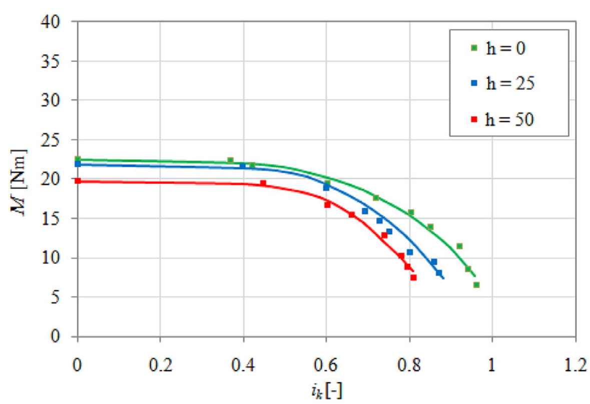

Fig.12. Dependence $M = f(i_k)$ for the gap $h > 0$, filling degree ψ = 92%, temperature T_2 = 60 - 80°C, velocity ω_1= 100 rad/s and right-hand rotations of the HC pump rotor

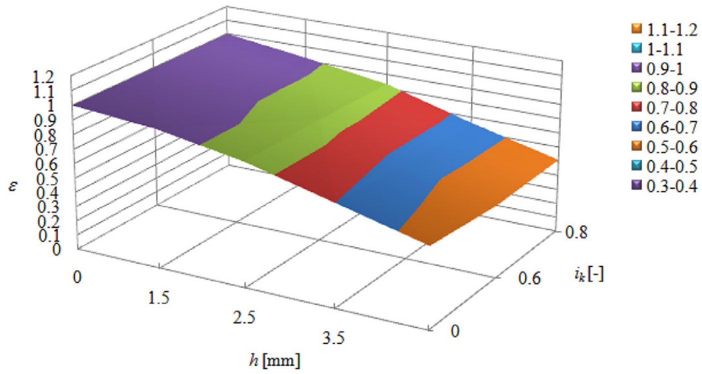

Fig. 13. Dependence $\varepsilon = f(i_k, h)$ for ω_1 = 100 rad/s and left-hand rotations of the pump rotor

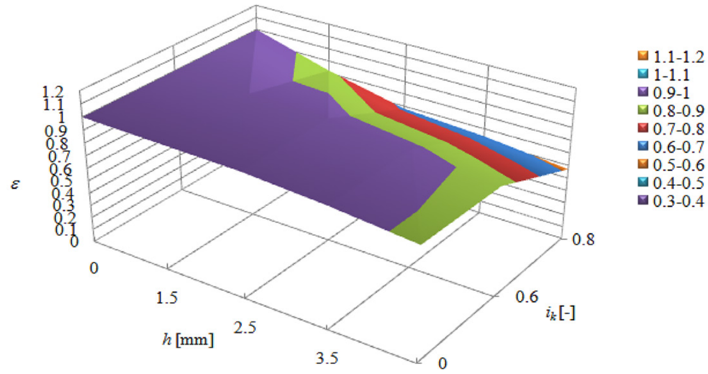

Fig. 14. Dependence $\varepsilon = f(i_k, h)$ for ω_1 = 100 rad/s and left-hand rotations of the pump rotor

both rotation directions of the pump rotor, assuming that the dependence is arbitrarily described by the following function:

$$\varepsilon = ai_k^2 + bi_k + ch^2 + dh + ei_k \cdot h + f \tag{34}$$

where: *a, b, c, d, e, f* – numerical coefficients.

The equations of planes $\varepsilon_{av} = f(h, i_k)$ for both rotation directions of the pump rotor, obtained as a result of these calculations, are shown in Table 10. The correctness assessment of the calculations of flow rate reduction coefficient ε is conducted on the basis of the errors δ_ε obtained for the torque value M_e and the torque value M_t. The values are calculated numerically on the basis of the mathematical model equations, with the use of the dependence $\varepsilon_{av} = f(h, i_k)$, in accordance with the contents of Table 10. Table 11 and Table 12 show the juxtaposed relative errors of the coefficient ε, the values of ε_{av} and the values ε_e obtained on the basis of the experiment for ω_1 = 100 rad/s and different rotation directions of the pump rotor.

Results of model calculations

Steady-state and dynamic calculations, concerning the control method of the wind power plant generator's drive system containing a HC controlled by sliding the turbine rotor, are carried out on the basis of the developed mathematical model and geometric data of the examined HC. The numerical calculations used an algorithm whose diagram is shown in Figure 15.

The input data for the algorithm were the parameters of the electric generator (angular velocity ω_2, torque M_l), HC parameters (blade angles β, radii *r*, density of the working fluid ρ, coefficient φ, coefficient ε) and the kinematic ratio i_k* for which the gap $h = 0$. The result of the calculations was the gape size *h* for the assumed angular velocity ω_w.

Steady-state calculations

The calculations are performed for three selected cases of the wind power plant's performance and for the HC operating as a controlled brake. For Case 1, the gear ratio for the gearbox *i* is selected so that the initial gap size *h* between the rotors would equal zero for ω_w = 1.0 rad/s, and the angular velocity of the turbine rotor ω_2 would equal 150 rad/s. It should be emphasized that (at the same velocity ω_w) the greater the mechanical power *P* supplied to the HC, the greater the gear ratio *i*, because $\omega_1 = \omega_w \cdot i$ and $P \approx \omega_1^3$. As the wind speed increases,

Table 10. Dependency equations $\varepsilon_{av} = f(h, i_k)$

Rotation direction of the pump rotor	Equation $\varepsilon_{av} = f(h, i_k)$
Left	$\varepsilon_{av} = 0.16 i_k^2 - 0.13 i_k - 0.0184 h^2 + 0.002 h - 0{,}01 i_k \cdot h + 1$
Right	$\varepsilon_{av} = -0.158 i_k^2 + 0.126 i_k - 0.0064 h^2 + 0.008 h - 0.013 i_k \cdot h + 1$

Table 11. Flow rate reduction coefficient errors ε_{av} for ω_1 = 100 rad/s and left-hand rotations of the pump rotor

ω_1 = 100 rad/s		ε_{av}			ε_e			δ_ε [%]		
		i_k			i_k			i_k		
		0	0.6	0.8	0	0.6	0.8	0	0.6	0.8
Gap *h* [mm]	0	1.00	0.98	1.00	1.00	1.00	1.00	0.00	2.04	0.00
	15	0.96	0.93	0.95	0.92	0.91	0.92	4.56	2.05	3.80
	25	0.89	0.85	0.87	0.89	0.83	0.83	0.00	3.35	5.47
	35	0.78	0.74	0.76	0.69	0.66	0.66	13.57	11.44	14.96
	50	0.55	0.50	0.51	0.55	0.50	0.51	0.00	0.00	0.00

Table 12. Flow rate reduction coefficient errors ε_{av} for ω_1 = 100 rad/s and right-hand rotations of the pump rotor

ω_1 = 100 rad/s		e_{av}			ε_e			δ_ε [%]		
		i_k			i_k			i_k		
		0	0.6	0.8	0	0.6	0.8	0	0.6	0.8
Gap *h* [mm]	0	1.00	1.00	1.00	1.00	1.00	1.00	0.00	0.00	0.00
	15	0.99	0.99	0.98	0.99	0.99	0.82	0.84	0.00	20.18
	25	0.98	0.98	0.95	0.98	0.98	0.68	0.00	0.00	39.93
	35	0.95	0.94	0.91	0.94	0.94	0.64	0.54	0.00	43.33
	50	0.88	0.86	0.83	0.88	0.86	0.57	0.00	0.00	45.73

the angular velocity of the rotor ω_w increases to ω_w = 2.0 rad/s. As a result, the size of the gap *h* increases. The calculation results for Case 1 are shown in Figure 16 and Figure 17.

For Case 2, the gear ratio for the gearbox *i* is selected so that the initial gap size *h* between the rotors would be greater than zero for ω_w = 1.5 rad/s, and ω_2 would equal 150 rad/s. As the wind speed increases, the angular velocity of the rotor increases from ω_w = 1.5 rad/s to ω_w = 2.0 rad/s, which resulted in a decrease in the size of the gap *h*. The calculation results for Case 2 are shown in Figure 18 and Figure 19.

For Case 3 it is assumed that the nominal working conditions of the generator occur, similarly to Case 2, for the wind power plant's turbine rotor speed ω_w = 1.5 rad/s. It is assumed that the gearbox has two selectable ratios, and ω_w varies from 1.0 rad/s to 2.0 rad/s. A higher ratio is selected for the velocity ω_w< 1.5 rad/s, while a lower ratio is selected for the velocity ω_w> 1.5 rad/s. The gear ratio is 1.6. When the rotations ω_w of the wind power plant's rotor exceed 1.5 rad/s, a lower gear ratio is selected, and the HC rotors gradually move aside from *h* = 0 to the maximal *h* value. The calculation results for Case 3 are shown in Figure 20 and Figure 21.

According to the sensitivity method [38], variation of the gap size δh caused by variation of angular velocity $\delta\omega_w$ can be estimated using the partial derivative $\delta h/\delta\omega_w$. Figure 22, for example, shows the dependencies of the derivative $\delta h/\delta\omega_w$ on the angular velocity ω_w for left-hand rotations of the pump rotor, obtained on the basis of Figure 16 and Figure 18, respectively.

When considering the use of the HC with a stopped turbine rotor as a hydrodynamic brake in the wind power plant, it is assumed that the gear ratio of the gearbox is *i* = 200 and the power plant's rotor angular velocity range is ω_w od 1.0 rad/s to 2.0 rad/s. The velocity of the pump rotor ω_1 is calculated from the formula: $\omega_1 = i \cdot \omega_w$, and then the braking torque M_h is determined for i_k = 0, for various values of the gap width *h* and both rotation directions of the HC pump rotor. The calculation results are presented in Figure 23 for left-hand rotations of the HC pump rotor, and in Figure 24 for right-hand rotations of the HC pump rotor.

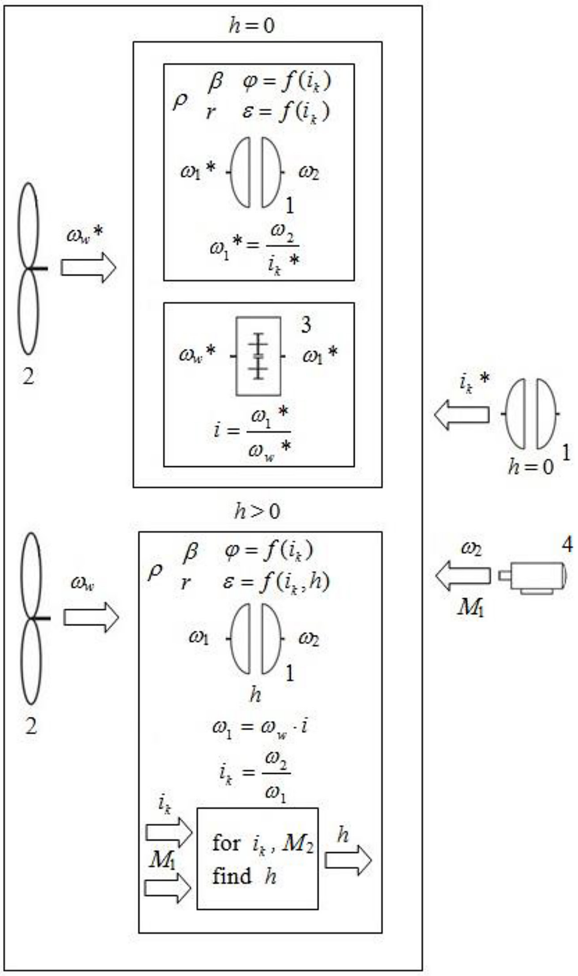

Fig. 15. Scheme of the algorithm used in numerical calculations: 1 – HC, 2 – rotor of wind power plant, 3 – gear box, 4 – electric generator

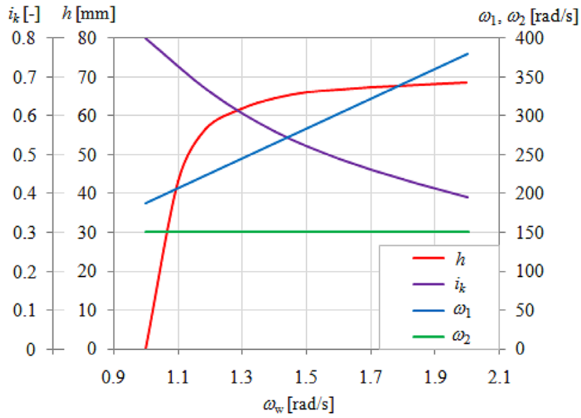

Fig. 16. Calculation results for Case 1 and left-hand rotations of the pump rotor for ω_2 = 150 rad/s and i = 190

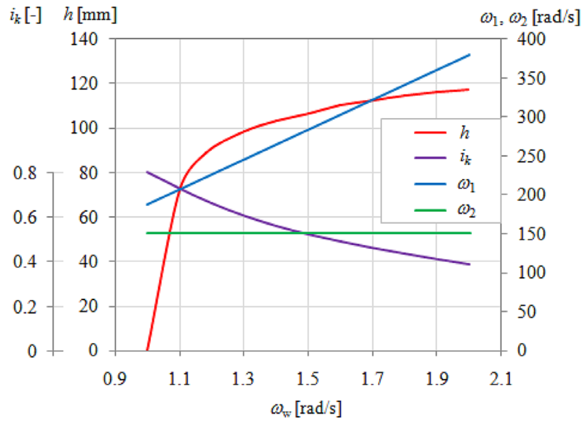

Fig. 17. Calculation results for Case 1 and right-hand rotations of the pump rotor for ω_2 = 150 rad/s and i = 190

Dynamic calculations

The dynamic calculations are performed numerically by solving equations (1) on the basis of the 4th Runge-Kutta-Gill method with a time step of 0.02 s, for two cases of constraints labelled as Case 4 and Case 5, causing transient motion of the wind power plant's drive system. The data for dynamic calculations are presented in Table 13.

It is assumed for Case 4, that the HC is not controlled, and the constraint is the jump of the driving torque M_s from 50 Nm to 200 Nm. As a result, the angular velocities of both rotors ω_1, ω_2 increase with time, as does the torque on the generator shaft M_r, as presented in Fig. 25.

In Case 5, it is assumed that the HC is controlled by sliding the turbine rotor, and the transient motion causes a jump in the angular velocity ω_1 of the HC input shaft from 190 rad/s to 360 rad/s, Fig. 26. As a result of the jump, the driving torque M_s rises instantly from 50 Nm to 200 Nm. However, as a result of the rotors sliding away from each other, it decreases to 50 Nm within 4 seconds, at which point the angular velocity ω_2 of the generator shaft is 150 rad/s.

Analysis of the results

The calculations for Case 1 presented in Fig. 16 and Fig. 17 show that HC control is performed by changing the speed ratio i_k from 0.39 to 0.80 by sliding the rotors. The rotors slide within the range from 0 to 70 mm for left-hand rotations and within the range from 0 to 118 mm for right-hand rotations. In the calculations for Case 2, the results of which are shown in Fig. 18 and Fig. 19, the gap $h \neq 0$, so the HC rotors slide away and towards each other. For the assumed gear ratio values, the control can occur within the ω_w ranges from 1.3 to 2.0 rad/s (for both rotation directions

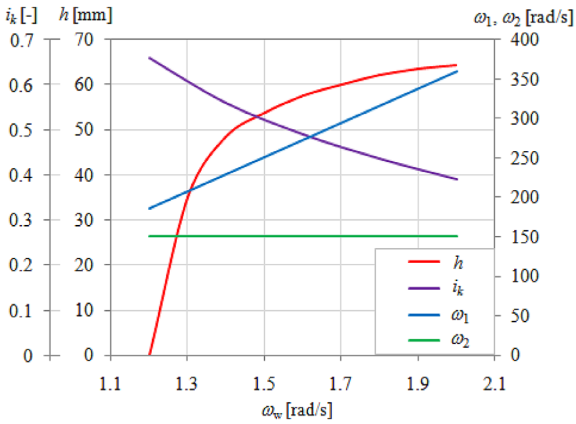

Fig. 18. Calculation results for Case2 and left-hand rotations of the pump rotor for ω_2 = 150 rad/s and i = 200

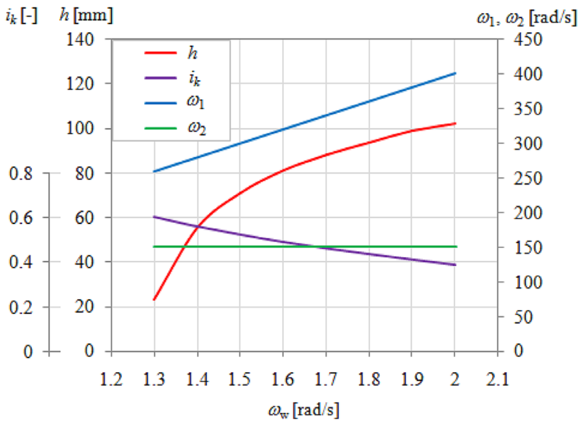

Fig. 19. Calculation results for Case 2 and right-hand rotations of the pump rotor for ω_2 = 150 rad/s and i = 200

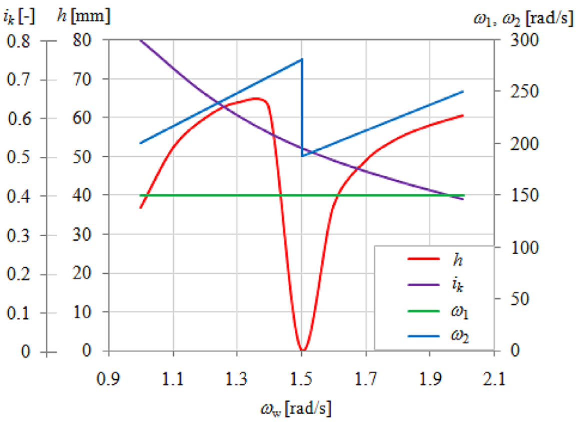

Fig. 20. Calculation results for Case 3 and left-hand rotations of the pump rotor for ω_2 = 150 rad/s and i = 200 or i = 125

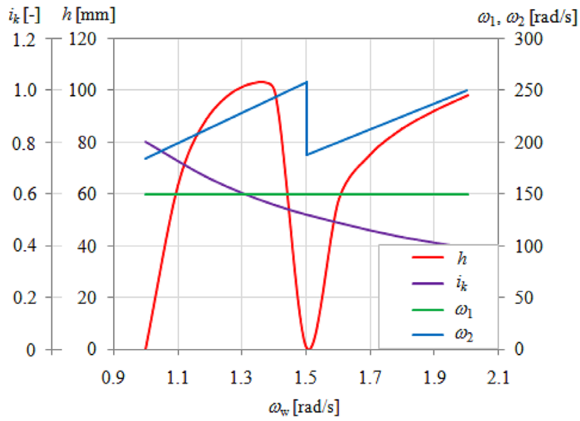

Fig. 21. Calculation results for Case 3 and right-hand rotations of the pump rotor for ω_2 = 150 rad/s and i = 185 or i = 125

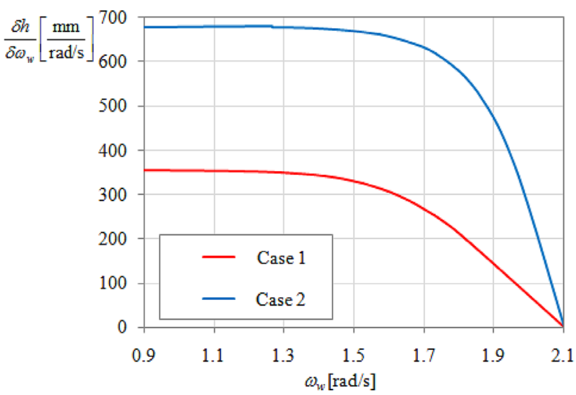

Fig. 22. Dependence of partial derivative $\delta h/\delta\omega_w$ on the angular velocity ω_w for left-hand rotations of the pump rotor

of the HC pump rotor) when the size of the gap between the rotors is smaller than 100 mm. The speed ratio i_k changes from 0.38 to 0.60. In Case 3, whose calculation results are presented in Fig. 20 and Fig. 21, the gear ratio i_k change occurs between 0.6 and 0.8, whereas the size changes of the gaps between rotors are 60 mm for the left-hand rotations and 100 mm for the right-hand rotations. Maximal sizes of the gap h depend slightly on the angular velocity ω_2 and the rotation direction of the pump rotor, wherein the right-hand rotations assume higher values. Based on Fig. 22, it can be seen that the relationships $\delta h/\delta\omega_w = f(\omega_w)$ for the two considered cases and left-hand rotations of the pump rotor have a similar course. With an increase in the angular velocity ω_w from 1.0 rad/s to 1.5 rad/s, the partial derivative $\delta h/\delta\omega_w$ is almost constant, and with a further increase in the angular velocity ω_w to 2 rad/s, it decreases to zero. Such a course of the partial derivatives $\delta h/\delta\omega_w$ means that the faster response of the control system to changes ω_w is occur for higher values

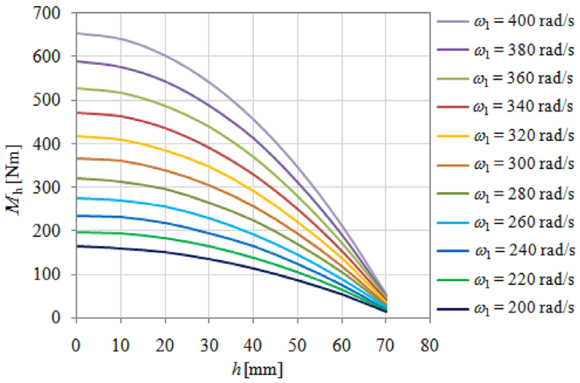

Fig. 23. Dependence of the braking torque M_h on the gap h for left-hand rotations of the HC pump rotor for different angular velocities of the pump rotor

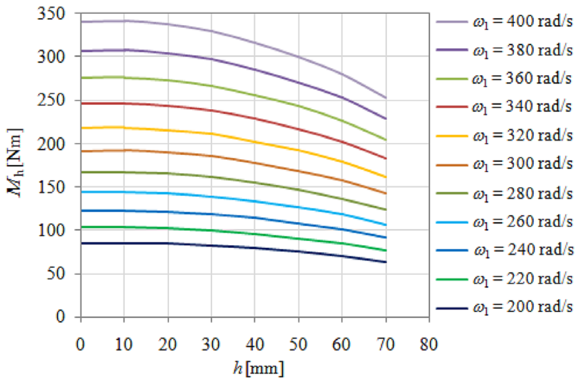

Fig. 24. Dependence of the braking torque M_h on the gap h for right-hand rotations of the HC pump rotor for different angular velocities of the pump rotor

Table 13. Transient motion calculation data

Starting point			Mass moments of inertia		Rotor sliding time
$M_{s0} = M_{r0}$	ω_{10}	ω_{20}	J_1	J_2	t_w
50 Nm	190 rad/s	150 rad/s	0.0399 kgm^2	0.0218 kgm^2	4 s

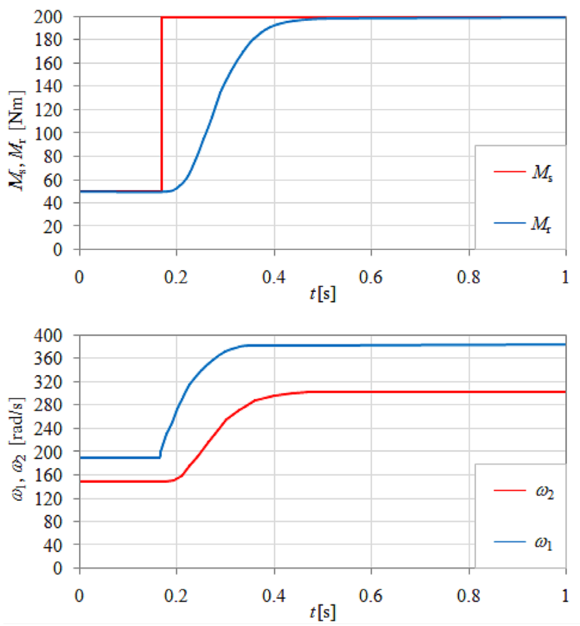

Fig. 25. The course of angular velocities ω_1, ω_2 and the torque M_r caused by the jump of M_s

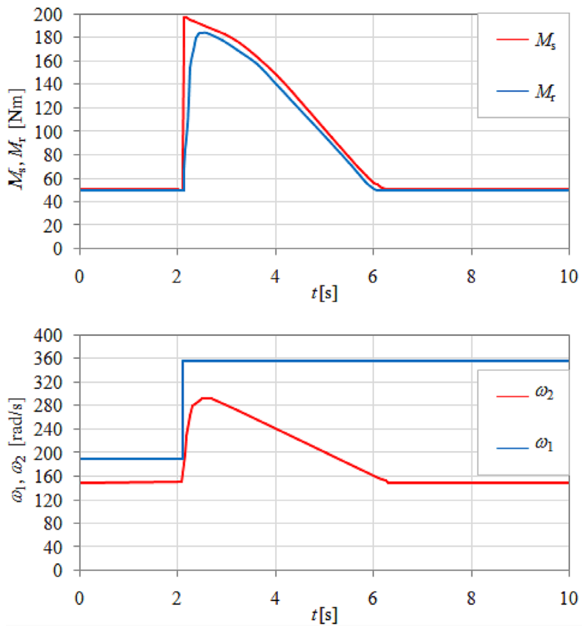

Fig. 26. The courses of angular velocity ω_2 and torques M_r, M_s caused by the jump of w_s

of the angular velocity ω_w. The comparison of the calculation results for Case 3 with the calculation results for Case 1 and Case 2 shows that the use of a gearbox with two selectable ratios between the rotor of the wind turbine and the HC enables HC operation at higher ratios i_k, and thus higher efficiencies and smaller gaps h.

On the basis of the charts shown in Fig. 23 and Fig. 24, it is noticeable that the maximal values of the braking torque M_h occur for $h = 0$ within the assessed range of the angular velocity ω_1 and range respectively from 163 Nm to 652 Nm for left-hand rotations of the HC pump rotor and 85 Nm to 340 Nm for right hand-rotations of the HC pump rotor. For the left-hand rotations of the HC pump rotor, the values of the braking torque M_h are approximately 2 times higher than for right-hand rotations. Increasing the gap value from 0 to 70 mm causes a fourfold decrease in the value of the braking torque M_h for both rotation directions of the HC pump rotor.

In Case 4, which concerns the transient motion of the HC caused by a jump in the driving torque value (as shown in Fig. 25), there is an increase of both ω_1 and ω_2 angular velocities in time, so it is not possible to maintain the angular velocity of the electric current generator's input shaft at 150 rad/s. Using the HC with sliding rotors for the jump in angular velocity ω_w, makes it possible to maintain the obtained value ω_2 = 150 rad/s after a transition period, as shown in Fig. 26. The duration of the transition period for the spreading time of the rotors equal to 4 s is 4.3 s, so it is proximate to the rotors' spreading time.

CONCLUSIONS

On the basis of the research results obtained from the performed numerical calculations based on the developed mode, the following conclusions are formulated:

The method of HC control by sliding rotor scan be successfully employed in the electric generator drive system in the wind power plant. It is supported by the fact, that a power excess often occurs on the rotor shaft of the wind power plant due to high-speed winds. This is significant because of the relatively low efficiency of the controlled HC.

The design of the HC controlled by increasing the distance between rotors is simple to implement. In the wind power plant containing a HC with sliding the turbine rotor, when the wind speed changes twice, it is possible to maintain a constant power of the generator by sliding the rotors within the range from 0 to 100 mm, when the speed ratio and the HC efficiency change from 0.4 to 0.8.

After the turbine rotor is stopped, the assessed HC can be successfully employed as a controlled hydrodynamic brake in the researched drive system of the wind power plant. This is due to the fact, that increasing the size of the gap between rotors up to 70 mm causes a fourfold decrease of the braking torque.

Essential design parameters of the HC controlled by increasing the distance between rotors are the angles of the rotor blades. A selection of blades can significantly influence the characteristics of the clutch. This is proven by significant differences in the torque values transferred for left-hand and right-hand rotations of the assessed HC's input shaft.

Errors of the developed mathematical model of the HC controlled by increasing the distance between rotors do not exceed the values of mathematical models in engineering calculations, usually accepted at 20%.

The obtained research results provide the basis for further theoretical and experimental research concerning the use of the HC control method by sliding rotors in hydrodynamic drive systems of other machines.

REFERENCES

1. Basak P., Chowdhury S., Halder nee Dey S., Chowdhury S.P. A literature review on integration of distributed energy resources in the perspective of control, protection and stability of microgrid. Renewable and Sustainable Energy Reviews 2012; 16(8): 5545-5556. https://doi.org/10.1016/j.rser.2012.05.043
2. Ramabhotla S. and Bayne B.S. Cost and availability optimization of wind energy with distributed energy resources of a microgrid. Wind Engineering 2019; 43(6): 559-572. https://doi.org/10.1177/0309524X18820019
3. Leary J. et al. Finding the niche: A review of market assessment methodologies for rural electrification with small scale wind power. Renewable and Sustainable Energy Reviews 2020; 133: 110240. https://doi.org/10.1016/j.rser.2020.110240
4. Ismaiel A. Wind turbine blade dynamics simulation under the effect of atmospheric turbulence. Emerging Science Journal 2023; 7(1): 162-176. https://doi.org/10.28991/ESJ-2023-07-01-012
5. Adanta D., Sari D.P., Syofii I., Prakoso A.P., Ade Saputra M.A., Thamrin I. Performance comparison of crossflow turbine configuration upper blade convex and curvature by computational method. Civil Engineering Journal 2023; 9(1): 154-165. http://dx.doi.org/10.28991/CEJ-2023-09-01-012
6. Tahiri F.E., Chikh K., Khafallah M. Optimal management energy system and control strategies for isolated hybrid solar-wind-battery-diesel power system. Emerging Science Journal 2021; 5(2): 111-124. http://dx.doi.org/10.28991/esj-2021-01262
7. Staudt L. Design and development of small wind turbines. WIT Transactions on State of the Art in Science and Engineering. WIT Press, 2010: 257-276.
8. Díaz-González F., Sumper A., Gomis-Bellmunt O., Villafáfila-Robles R. A review of energy storage technologies for wind power applications. Renewable and Sustainable Energy Reviews 2012; 16(4): 2154-2171. https://doi.org/10.1016/j.rser.2012.01.029

9. Apostolou D. and Enevoldsen P. The past, present and potential of hydrogen as a multifunctional storage application for wind power. Renewable and Sustainable Energy Reviews 2019; 112: 917-929. https://doi.org/10.1016/j.rser.2019.06.049
10. Blaabjerg F., Liserre M., Ma K. Power electronics converters for wind turbine systems. IEEE Transactions on Industry Applications 2012; 48(2): 708-719. https://doi.org/10.1109/TIA.2011.2181290
11. Hippel S., Jauch C., Ritschel U. Hydraulic-pneumatic flywheel configurations for controlling the inertia of a wind turbine rotor. Wind Engineering 2019; 43(2): 114-132. https://doi.org/10.1177/0309524X18780386
12. Hocine L., Menaa M., Yazid K. Sensorless control of wind power generator with flywheel energy storage system. Wind Engineering 2021; 45(2): 257-277. https://doi.org/10.1177/0309524X19884709
13. Müller H. et al. Grid compatibility of variable speed wind turbines with directly coupled synchronous generator and hydro-dynamically controlled gearbox. In 6th International Workshop on Large-Scale Integration of Wind Power and Transmission Networks for Offshore Wind Farms, Delft, Netherlands, 2006, 307-315.
14. Rommel D.P., Maio D.D., Tinga T. Calculating loads and life-time reduction of wind turbine gearbox and generator bearings due to shaft misalignment. Wind Engineering 2021; 45(3): 547-568. https://doi.org/10.1177/0309524X20914022
15. Lopes J.J.A., Vaz J.R.P., Mesquita A.L.A., Blanco C.J.C. An approach for the dynamic behavior of hydrokinetic turbines. Energy Procedia 2015; 75: 271-276. https://doi.org/10.1016/j.egypro.2015.07.334
16. Lunney E., Ban M., Duic N., Foley A. A state-of-the-art review and feasibility analysis of high altitude wind power in Northern Ireland. Renewable and Sustainable Energy Reviews 2017; 68(2): 899-911. https://doi.org/10.1016/j.rser.2016.08.014
17. WinDrive. Voith Turbo. Information brochure nr cr606en, 2009.
18. Brun K., Meyenberg C., Thorp J., Kurz R. Hydrodynamic torque converters for oil and gas compression and pumping applications: basic principles, performance characteristics and applications. In 44th Turbomachinery and 31st Pump Symposia, Houston, Texas, 2015, 1-14.
19. Stesin S.P. Blade machines and hydrodynamic torque converters. Machinostrjenie, 1990 (in Russian).
20. Weston E.B. Theory and design of automotive transmission components. Butterworth, 1967.
21. Clements H.A. Stopping and reversing high power ships. The American Society of Mechanical Engineers 1994; 89-GT-231: 1-11. https://doi.org/10.1115/89-GT-231
22. Olszak A., Osowski K., Kęsy Z., Kęsy A. Modelling and testing of a hydrodynamic clutch filled with electrorheological fluid in varying degree. Journal of Intelligent Material Systems and Structures 2019; 30(4): 649-660. https://doi.org/10.1177/1045389X18818780
23. Olszak A., Osowski K., Kęsy Z., Kęsy A. Investigation of hydrodynamic clutch with MR fluid. Journal of Intelligent Material Systems and Structures 2019; 30(1): 155-168. https://doi.org/10.1177/1045389X18803463
24. Madeja J., Kęsy Z., Kęsy A. Application of ER fluid in hydrodynamic clutch. Smart Materials and Structures 2011; 20: 105005. https://doi.org/10.1088/0964-1726/20/10/105005
25. Kotliński J. et al. Fabrication of hydrodynamic torque converter impellers by using the selective laser sintering method. Rapid Prototyping Journal 2013; 19(6): 430-436. https://doi.org/10.1108/RPJ-04-2011-0043
26. Kęsy A. and Kotliński J. Mechanical properties of parts produced by using polymer jetting technology. Archives of Civil and Mechanical Engineering 2010; 10(3): 37-50. https://doi.org/10.1016/s1644-9665(12)60135-6
27. Kotlinski J., Kęsy Z., Kęsy A., Jackson M., Parkin R. Dimensional deviations of machine parts produced in laser sintering technology. International Journal of Rapid Manufacturing 2009; 1(1): 88-98. https://doi.org/10.1504/ijrapidm.2009.028933
28. Ishihara T.A study of hydraulic torque converter. Report of University of Tokyo 1955; 5: 150-202.
29. Hrovat D. and Tobler W. Bond graph modelling and computer simulation of automotive torque converters. Journal of the Franklin Institute 1985; 319(1-2): 93-114. https://doi.org/10.1016/0016-0032(85)90067-5
30. Jaschk P. Mathematische modellierung des betriebs verhaltens hydrodynamischer kupplungen mit hybriden modell ansätzen. Mitteilungen aus dem Institut für Mechanik, 2000.
31. Andersson S. On hydrodynamic torque converters. Transactions of Machine Elements Divison. Lund Technical University Lund Sweden, 1982.
32. Jung J. H., Kang S., Hur N. A numerical study of a torque converter with various methods for the accuracy improvement of performance prediction. Progress in Computational Fluid Dynamics, an International Journal 2011; 11(3-4): 261-268. https://doi.org/10.1504/PCFD.2011.041027
33. Luo Y., Zuo Z.G., Fan H.G., Zhung W.L. Numerical simulation of the two-phase flows in a hydraulic coupling by solving VOF model. IOP Confer-

ence Series: Materials Science and Engineering 2013; 52: 072022. http://dx.doi.org/10.1088/1757-899X/52/7/072022

34. Schweitzer J. and Gandham J. Computational fluid dynamics in torque converter: validation and application. International Journal of Rotating Machinery 2003; 9: 411-418. https://doi.org/10.1155/S1023621X03000393
35. Liu C. et al. Large eddy simulation for improvement of performance estimation and turbulent flow analysis in a hydrodynamic torque converter. Engineering Applications Computational Fluid Mechanics 2018; 12(1): 635-651. https://doi.org/10.1080/19942060.2018.1489896
36. Kęsy A. and Kęsy Z. Damping characteristics of a transmission system with a hydrodynamic torque converter. Journal of Sound and Vibration 1993; 163(3): 493-506. https://doi.org/10.1006/jsvi.1993.1308
37. Murin J. A machine aggregate with hydrodynamic power transmission at periodic loading. Mechanism and Machine Theory 2001; 36(1): 77-92. https://doi.org/10.1016/S0094-114X(00)00029-X
38. Kęsy Z. and Kęsy A. Application of sensitivity methods to the improvement of a hydrodynamic torque converter manufacturing process. International Journal of Computer Applications in Technology 1993; 6(1): 35-38. https://doi.org/10.1504/IJCAT.1993.062612
39. Kęsy Z. and Kęsy A. Computer–aided method to calculate coefficients in dynamic equations for multi–element torque converter. International Journal of Vehicle Design 1992; 13(2): 134-143. https://doi.org/10.1504/IJVD.1992.061718
40. Behrens H., Jaschke P., Steinhausen J., Waller H. Modeling of technical systems: Application to hydrodynamic torque converters and couplings. Mathematical and Computer Modelling of Dynamical Systems 2000; 6(3): 223-250. https://doi.org/10.1076/1387-3954(200009)6:3;1-I;FT223
41. Kubo M., Ejiri E., Kumada H., Ishii Y. Improvement of prediction accuracy for torque converter performance: One-dimensional flow theory reflecting the stator blade geometry 1994; JSAE Review. 15(4): 309-314. https://doi.org/10.1016/0389-4304(94)90212-7
42. Kęsy A. and Kądziela A. Construction optimization of hydrodynamic torque converter with application of genetic algorithm. Archives of Civil and Mechanical Engineering 2011; 11(4): 905-920. https://doi.org/10.1016/s1644-9665(12)60086-7
43. Vaz J.R.P., Wood D.H., Bhattacharjee D., Lins E.F. Drivetrain resistance and starting performance of a small wind turbine. Renewable Energy 2018; 117: 509-519. https://doi.org/10.1016/j.renene.2017.10.071
44. Farias G.M., Galhardo M.A.B., Vaz J.R.P., Pinho J.T. A steadystate based model applied to small wind turbines. Journal of the Brazilian Society of Mechanical Sciences and Engineering 2019; 41: 209. https://doi.org/10.1007/s40430-019-1704-0
45. Fu L., Wei Y., Fang S., Tian G., Zhou X. A wind energy generation replication method with wind shear and tower shadow effects. Advances in Mechanical Engineering 2018; 10(3): 1-11. https://doi.org/10.1177/1687814018759216
46. Adibi Asl H., Azad N.L., McPhee J. Math-based torque converter modelling to evaluate damping characteristics and reverse flow mode operation. International Journal of Vehicle Systems Modelling and Testing 2014; 9(1): 36-55. https://doi.org/10.1504/IJVSMT.2014.059155
47. Adibi Asl H., Azad N.L. and McPhee J. Modeling torque converter characteristics in automatic drivelines: Lock-up clutch and engine braking simulation. In: Proceedings of the ASME 2012 International Design Engineering Technical Conferences and Computers and Information in Engineering Conference. International Conference on Advanced Vehicle Technologies, Chicago, Illinois, USA, 2013, 359-367.
48. Szczepaniak C., Kęsy A., Kęsy Z. Damping performance of power transmission system with hydraulic torque converter. Vehicle System Dynamics 1991; 20(5): 283-295.
49. Kęsy Z. and Kęsy A. Dynamic aspects of a hydrodynamic torque converter working in a transmission system. Machine Vibration 1995; 4: 152-160.
50. Ishihara T. and Emori R.I. Torque converter as a vibrator damper and its transient characteristics. SAE Technical Paper 1966; 660368. https://doi.org/10.4271/660368
51. Whitfield A., Wallace F.J., Patel A. Design of three element hydrokinetic torque converters. International Journal of Mechanical Sciences 1983; 25(7): 485-497. https://doi.org/10.1016/0020-7403(83)90041-3
52. Kotwicki A.J. Dynamic models for torque converter equipped vehicles. SAE Technical Paper 1982; 820393. https://doi.org/10.4271/820393
53. Kęsy Z. Hydrodynamic torque converter controlled by properties of working fluid. Politechnika Radomska, 2003 (in Polish).
54. Jandasek V.J. The design of a single-stage three-element torque converter. SAE Technical Paper 1961; 610576. https://doi.org/10.4271/610576
55. Iwanicki W. et al. Experimental research concerning hydrodynamic clutches controlled by increasing distance between rotors. Advances in Science and Technology Research Journal 2021; 15(1): 218-229. https://doi.org/10.12913/22998624/132214